Rotational synchronization of camphor ribbons

Jyoti Sharma, Ishant Tiwari, Dibyendu Das, and P. Parmananda
Department of Physics, Indian Institute of Technology, Bombay, Powai, Mumbai 400 076, India

V. S. Akella
Department of Applied Mechanics, Indian Institute of Technology, Madras, Adyar, Chennai, Tamil Nadu 600036, India

Véronique Pimienta
Laboratoire des IMRCP, Université de Toulouse, CNRS UMR 5623, Université Paul Sabatier, 118 route de Narbonne 31062, Toulouse Cedex 9, France

(Received 27 March 2018; revised manuscript received 28 November 2018; published 7 January 2019)

Experiments on interacting pinned self-propelled rotators are presented. The rotators are made from paper with camphor infused in its matrix. The ribbons rotate due to Marangoni effect driven forces arising by virtue of surface tension gradients. Two such self-rotating camphor ribbons are observed to experience a repulsive coupling via the camphor layer in the common water medium. Lag synchronization in both corotating (same sense of rotation) and counterrotating (opposite sense of rotation) ribbons is reported for the experiments. This synchronization is found to be dependent on the pivot to pivot distance l. For distances less than the span of both the ribbons, l_c, the rotators successfully synchronize. Furthermore, it is experimentally perceived that synchronization in the counterrotating ribbons is more robust than in the corotating ribbons. We rationalize the mechanism of this synchronization via a theoretical model involving a Yukawa type interaction which is analyzed numerically.

DOI: 10.1103/PhysRevE.99.012204

I. INTRODUCTION

Synchronization is the rhythmic behavior of two or more *coupled* oscillators [1]. It is a widely studied phenomenon in nonlinear dynamics. It has been observed in a plethora of living and nonliving systems. In various chemical and physical systems like the Mercury beating heart [2–4], the electrochemical dissolution of metals [5–7], and the Josephson junction [8,9], fingerprints of synchronization have been reported. Recently, synchronization in filaments oscillating on the water surface has also been reported [10]. Synchronization found in biological systems has been extensively discussed in [11–16]. The coupling required for observing synchronization can be broadly classified into four categories, namely, mechanical, chemical, electrical, and biological coupling. For instance, pendula and metronomes couple mechanically via a common support or a spring [17,18], while oscillating reactions like the Belousov-Zhabotinsky reaction are coupled chemically [19]. Brain activity, heart signals, and power grids exhibit synchronized activity through electrical coupling [1,8]. Finally, coherent flashing of fireflies and the synchronization of the circadian rhythm to the day and night cycles would belong to the biological coupling scenario [8].

In this work, we report the synchronized rotational motion of two chemically coupled self-propelled camphor dipped paper ribbons on a liquid surface. The self-propelled motion (SPM) of camphor on the water surface has been studied extensively both experimentally and theoretically [20–23]. The driving force for this SPM of camphor is the surface tension imbalance induced by an asymmetric camphor layer surrounding the solid. It was first explained by Van der Mensbrugghe in 1869 [24]. Camphor is a promising candidate to make autonomous motors and to study the active particles' collective behaviors such as jamming [25]. Self-propelled entities made up of camphor show translational, rotational, and intermittent motion [26]. This motion depends on the size of the container, the shape of the particle, surface tension, and the temperature of the water medium [21]. It is sensitive to the boundary conditions of the enclosure [27], its chemical environment [28], and the distribution of the camphor layer on the water surface.

The camphor layer formed around the particles can serve as a coupling medium when two or more particles are at play [21]. Exploring this, Nakata and co-workers have reported synchronized motion of two camphor boats in a single [29] and dual [30] circular annular channel, as well as in triangular and square channels [31]. In addition, synchronization of the water flow around two fixed camphor disks [32] has also been observed.

While translational synchronization of two camphor boats in closed channels of various shapes has been studied [29,31], rotational synchronization remains unexplored. However, rotational synchronization of corotating and counterrotating Landau-Stuart and Rossler oscillators has been numerically reported [33]. Camphor particles can rotate either due to the asymmetry in their shape [21] or by spontaneous symmetry breaking [34]. There is a control on the direction of rotation, i.e., either clockwise or counterclockwise in the former case (shape chirality), but there is no such control in the latter scenario (symmetry breaking of the surroundings). Analytically,

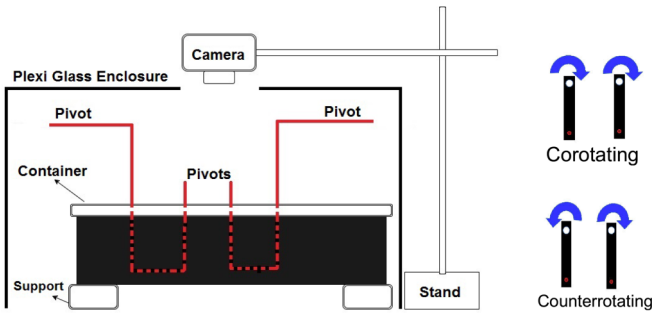

FIG. 1. The schematic side view of the experimental setup (left) and the upper view of the camphor ribbons (right). The white (upper) dots in the ribbons (right) are used to track the ribbon trajectories, while the red (lower) dots indicate the position of the pivot points.

the rotational motion due to spontaneous symmetry breaking is understood only for the elliptical camphor particles [35].

In this work, to allow only rotational motion, the camphor ribbons have been pivoted about a thin wire. Once the ribbon touches the water surface, a camphor layer forms around it. Ideally, this camphor layer around the ribbon should be symmetric and uniform, leading to no motion of the ribbon. But due to both the small irregularities in the shape of the ribbon and the initial local fluctuations in the camphor concentration around it this symmetry is broken. Hence, the camphor ribbons employed in our experiments rotate due to spontaneous symmetry breaking [34]. The ribbons are coupled *indirectly* [36] via the camphor layer on the common water surface.

For coupled rotators, various types of synchronization have been observed in previous numerical works. For example, mirror synchronization involves the rotators being synchronized such that they are mirror images of one another [17]. Another example is the phenomenon of mixed synchronization, a term coined by Prasad [33], where one of the dynamical variables is in phase, while the other is antiphase synchronized. In our experiments, in-phase and mirror [17] synchronizations are observed for corotating and counterrotating ribbons, respectively. We have theoretically modeled the experimental observations using a repulsive Yukawa potential between two point oscillators constrained to move on a circle.

The paper is divided into six sections. In Sec. I, we have introduced the system along with a brief literature review. The experimental setup and results are presented in Secs. II and III, respectively. The simulation model and numerical results are described in Secs. IV and V. Finally, in the last section, a brief discussion of the work is presented.

II. EXPERIMENTAL PROTOCOL

The experiments were performed in a glass container of dimensions $25 \times 25 \times 4$ cm^3, placed inside a Plexiglas enclosure to prevent air drafts from interfering with the system. Figure 1 shows the schematic diagram of the experimental setup (left) and a sketch of co- and counterrotating camphor ribbons (right). The glass container is filled up to a height of 2 cm with deionized water at room temperature. A high speed video camera (GOPRO Hero-4, frame rate 120 Hz, 720 p resolution) is installed above the glass box to record the rotator dynamics.

Two rectangular paper ribbons of dimensions 2.0×0.4 cm^2 were cut out from the paper sheet. The ribbons were kept black in color with a white circular region at one end to aid with the motion tracking of the rotators [Fig. 1(b)]. Subsequently, they were dipped in a solution of 1.55 g laboratory grade camphor and 3.0 ml ethanol at room temperature. The ribbons were then left to dry in the air. After the ethanol had dried off from the ribbons, they were pivoted on a thin wire. Finally, they were placed on the surface of the water to observe their rotational motion.

We define twice the length of a ribbon (2×2.0 cm $= 4.0$ cm) as l_c. The pivot to pivot distance between the two ribbons is defined as l. Initially, the ribbons were kept at a pivot to pivot distance ($l > l_c$) and then were gradually moved towards each other until $\frac{l_c}{2} < l < l_c$.

The camphor ribbon rotates either in the clockwise or the counterclockwise direction depending upon the initial fluctuations. Hence, the initial sense of rotation is chosen at random by the ribbon. Although the initial direction of rotation is decided randomly, one can choose the desired rotational direction by externally perturbing the ribbons. When the two ribbons rotate in the same rotational sense, they are referred to as corotating while they are called counterrotating if they rotate in opposite directions [33].

The experimental videos (see the Supplemental Material [37]) have been analyzed using the MATLAB particle tracking code developed by Blair and Dufresne [38] based on the particle tracking algorithms of Crocker and Grier [39]. The positions of the white dots on the black ribbons is defined as (x_i, y_i). It was tracked using the aforementioned algorithm. For brevity, we refer to the positions of these white dots as the positions of the ribbons itself throughout this paper. For each scenario (unsynchronized, corotating, and counterrotating synchronized), the data have been recorded and analyzed for 60 s (7200 frames $\approx$ 48 rotations), out of which a suitable portion is presented.

III. RESULTS

As previously mentioned, the ribbons are coupled via the camphor layer in the common water medium. This coupling depends upon the pivot to pivot distance l. In Fig. 2, when the ribbons are kept at a distance $l > l_c$, there is very little coupling between them; hence the rotators remain unsynchronized [Figs. 2(a) and 2(b)]. However, for $l < l_c$, their rotations synchronize both for the corotating [Figs. 2(c) and 2(d)] and for the counterrotating [Figs. 2(e) and 2(f)] scenarios. It needs to be emphasized that there is a slowdown of oscillations from the unsynchronized [Figs. 2(a) and 2(b)] to the synchronized [Figs. 2(c)–2(f)] domain. However, this slowdown of oscillations is not related to synchronization. This decrease of the angular frequency as time progresses is also observed when ribbons are unsynchronized ($l > l_c$). This is not due to different arrangements of the ribbons in unsynchronized and synchronized scenarios or the coupling effects on the rotation speed but because of the intrinsic decrease of the angular frequency as time progresses. We believe that this slowdown of rotation is because of the depletion of camphor from the

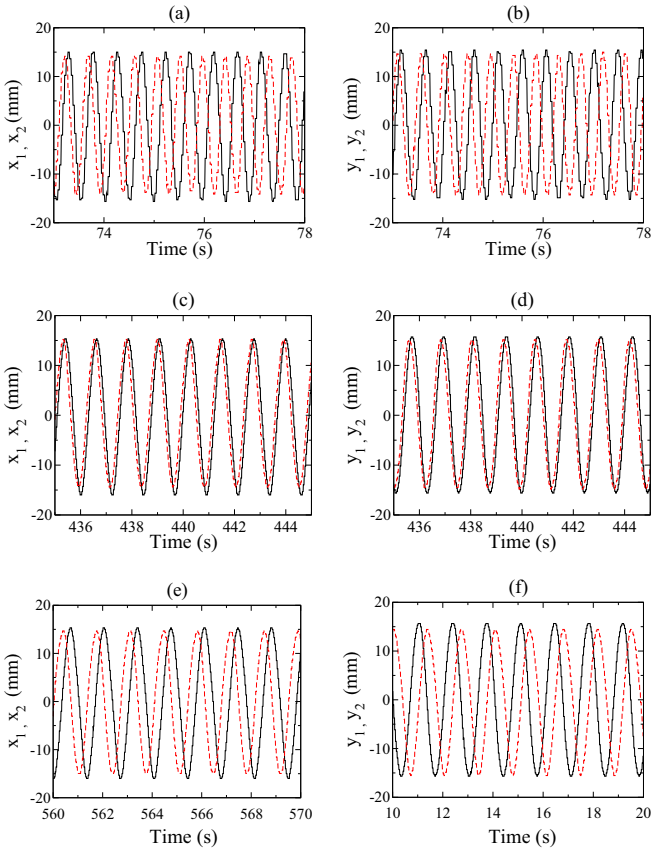

FIG. 2. Time variation of x position (left) and y position (right) of the ribbons for (a), (b) unsynchronized, (c), (d) corotating, and (e), (f) counterrotating scenarios. Red (dotted line) and black (solid line) curves represent the positions of the first and second ribbons, respectively. At a distance larger than l_c both x and y positions of the ribbons are unsynchronized with respect to each other but, while at a distance less than l_c, both x and y positions are lag synchronized for the corotating as well as for the counterrotating scenario. The slowdown of rotations as one goes from unsynchronized (top) to counterrotating (bottom) is due to the depletion of camphor from the ribbons and the gradual decrease in surface tension gradients as time progresses.

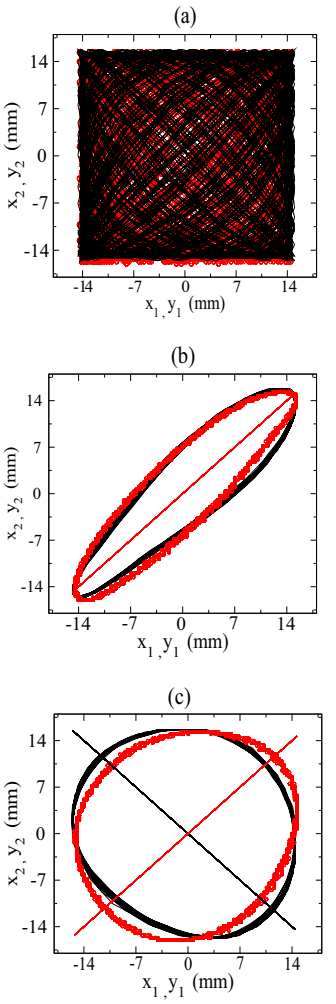

FIG. 3. Phase portraits of (a) unsynchronized, (b) corotating, and (c) counterrotating camphor ribbons. Data for 60 s are plotted for each panel. Red (circles) and black (solid) curves represent the x and y positions of the ribbons, respectively. The line of slope 1 (red) and of slope -1 (black) are drawn for reference. (a) All the available phase space is filled, indicating unsynchronized dynamics. (b) Both x and y positions are synchronized in phase with a constant phase lag for corotating ribbons. (c) For counterrotating ribbons the x and y positions are respectively in and out of phase synchronized. This type of synchronization is termed mirror synchronization [17].

ribbons compounded with the accumulation of camphor on the water surface. This lowers the surface tension gradients which drive the motion of the ribbons [40]. The mode of synchronization (co- or counterrotating) sets in depending on whether the rotators were brought closer while rotating in the same or in the opposite sense. Lag synchronization in x and y positions of the ribbons was observed for both corotating [Figs. 2(c) and 2(d)] and counterrotating [Figs. 2(e) and 2(f)] camphor ribbons. It is interesting to note that counterrotating ribbons have a larger constant phase difference with respect to each other in comparison to the corotating ribbons. Phase portraits shown in Fig. 3 for unsynchronized [Fig. 3(a)], corotating [Fig. 3(b)], and counterrotating [Fig. 3(c)] ribbons validate these observations. The corresponding videos (unsynchronized.mp4, co_rotating.mp4, and counter_rotating.mp4 are provided in the Supplemental Material [37].

In the case of corotating synchronization, both the x and the y positions of the ribbons change in a phase synchronized fashion with a constant phase difference close to zero. For counterrotating ribbons, out of phase synchronization is observed for the y coordinate of the ribbons' positions while the x coordinates vary in phase with each other. This observation has been previously termed mirror synchronization [17].

For a pivot to pivot distance $l < l_c$, if the ribbons come in physical contact, the rotators exhibit some transient dynamics followed by counterrotating synchronization as the preferred mode. This indicates that the counterrotating synchronization has a larger basin of attraction than that of its corotating counterpart. However, upon carefully moving two unsynchronized corotating ribbons closer while ensuring that there is no physical contact between the ribbons, one can observe a corotating mode of synchronization when the distance is less than l_c. Both modes of synchronization (corotating and

counterrotating) can been observed without the physical contact between the ribbons [41]. We have observed both corotating and counterrotating modes of synchronization for more than 400 cycles (1 cycle = 1.2 s) in the experiments.

IV. SIMULATION MODEL

To model the two ribbons, we have considered two point particles of unit mass constrained to move on a unit circle. It can be considered that the centers of the unit circles represent the pivot points for each ribbon. The pivots are kept at the origin (0,0) and (l,0). Therefore, the distance between the two pivots is $\boldsymbol{l}$. The angular positions of the particle with respect to its constraining unit circle can be defined as $\theta_1(t)$ and $\theta_2(t)$, respectively. Then the positions of the particles with respect to the common origin in the Cartesian coordinate system are $\vec{r}_1(t) = (\cos\theta_1(t), \sin\theta_1(t))$ and $\vec{r}_2(t) = (l + \cos\theta_2(t), \sin\theta_2(t))$, respectively.

The experimentally observed repulsive coupling between the camphor ribbons [25,42] is represented through a repulsive Yukawa type potential ($\frac{e^{-Kr}}{r}$) with a range determined by K. The Yukawa type interaction has been employed previously in a numerical study on an ensemble of self-propelled rods getting trapped in a wedge shaped boundary [43]. At any time t, for a distance $r(t) = |\vec{r}_1(t) - \vec{r}_2(t)|$ between the point particles, the Yukawa potential is $V_{\text{Yukawa}}(t) = \frac{e^{-Kr(t)}}{r(t)}$. From the potential, the force is $\frac{e^{-Kr(t)}}{r(t)^2}(1 + Kr(t))$, which determines the particle dynamics. The radial component of the Yukawa force is assumed to be balanced by the pivot constraint force. Therefore, only the tangential component of the force acts on the particles. This tangential component can be written as

$$(F_T(t))_1 = \frac{e^{-Kr(t)}}{r(t)^3}(1 + Kr(t))(\sin(\theta_1(t) - \theta_2(t)) + l\sin\theta_1(t)), \quad (1)$$

$$(F_T(t))_2 = \frac{e^{-Kr(t)}}{r(t)^3}(1 + Kr(t))(\sin(\theta_2(t) - \theta_1(t)) - l\sin\theta_2(t)). \quad (2)$$

This gives us the dynamical equations for the particles as $\ddot{\theta}_1(t) = (F_T(t))_1$ and $\ddot{\theta}_2(t) = (F_T(t))_2$, since the particles are of unit mass and the circle is of unit radius. Denoting the natural rotational frequencies of the first and second particles as ω_1 and ω_2, the dynamical equations can be written as two first order equations:

$$\dot{\theta}_1(t) = \omega_1(t), \quad (3)$$

$$\dot{\omega}_1(t) = (F_T(t))_1, \quad (4)$$

$$\dot{\theta}_2(t) = \omega_2(t), \quad (5)$$

$$\dot{\omega}_2(t) = (F_T(t))_2. \quad (6)$$

V. NUMERICAL RESULTS

We have simulated the dynamical equations (3)–(6) using the Runge-Kutta fourth order algorithm with a time step of 10^{-4}. After removing the transients for 1000 time units (1 time unit = 10^4 time steps), the system is set to evolve for another 1000 time units. The pivot to pivot distance is $l = 1.5$ units (for synchronized dynamics) and 6.5 units (for unsynchronized dynamics). The parameter K was kept fixed at 1.5 units. For the corotating scenario, the initial angular frequencies were taken to be $\omega_1 = 2.0$ and $\omega_2 = 2.05$, while they were taken as $\omega_1 = 2.0$ and $\omega_2 = -2.05$ in the counterrotating case. This frequency mismatch was introduced keeping in mind that the rotators in the experiments cannot be made completely identical. Initial phases of the particles were taken as $\theta_1 = \pi$ and $\theta_2 = \pi + 0.01$ for both the cases.

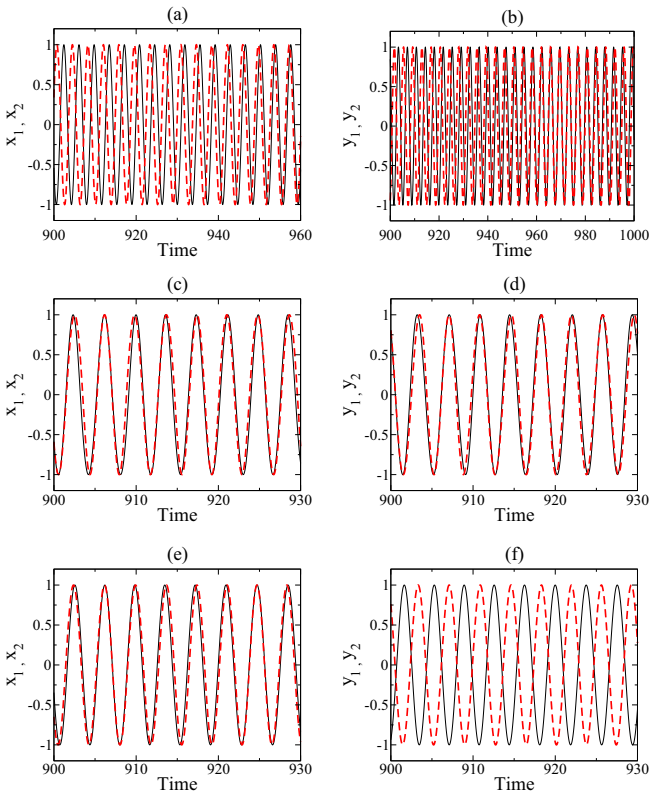

FIG. 4. Time variation of x position (left) and y position (right) of (a), (b) unsynchronized, (c), (d) corotating, and (e), (f) counterrotating particles. Red (dotted line) and black (solid line) curves represent the positions of the first and second particles, respectively. $x_i = \cos\theta_i$ and $y_i = \sin\theta_i$ for $i = 1, 2$. Cosines of the phase of the particles are synchronized in phase for both (c) corotating and (e) counterrotating particles. In contrast, the y positions synchronize (d) in phase for the corotating particles and (f) out of phase for the counterrotating particles.

Figures 4 and 5 show the simulation results for the corotating and the counterrotating particles. The cosine (sine) of their phases is analogous to the x (y) position of the ribbons in the experiments. For $l = 6.5$ units, the dynamics of the two particles remain unsynchronized [Figs. 4(a), 4(b), and 5(a)]. For $l = 1.5$ units, it can be observed that the cosines of the particles' phases synchronize in phase with each other for both the corotating [Fig. 4(c)] and the counterrotating scenarios [Fig. 4(e)]. However, the sine of each particle's phase synchronize in phase for the corotating [Fig. 4(d)] and

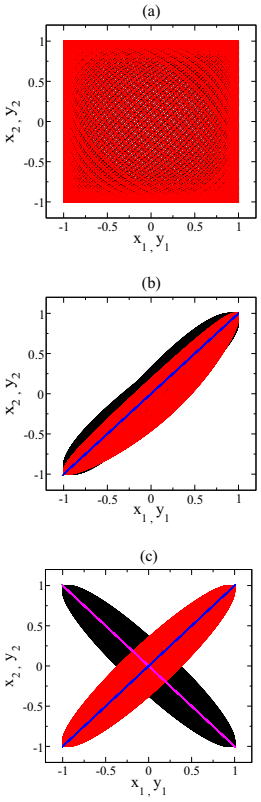

FIG. 5. Phase portraits of (a) unsynchronized, (b) corotating, and (c) counterrotating particles. Red and black curves represent the x and y positions of the particles, respectively. The line of slope 1 (blue) and of slope -1 (magenta) are drawn for reference. (c) The red curve and the black curve are along the line of slope 1 and -1, respectively. (a) All the available phase space is filled, indicating unsynchronized dynamics. (b) Both x and y positions are synchronized in phase with a constant phase lag for corotating particles. (c) For counterrotating ribbons, x and y positions are respectively in and out of phase synchronized. This is termed mirror synchronization [17].

out of phase for the counterrotating [Fig. 4(f)] particles. The phase plots [Fig. 5(b)] depict in-phase synchronization of both the cosine and the sine of the phase for the corotating particles. Therefore, the numerical model is able to capture the essence of the experimental observations. However, unlike the experiments, the particles do not get synchronized with a constant phase difference [compare Figs. 3(b) and 3(c) and Figs. 5(b) and 5(c)], nor do they experience a slowdown in their angular frequencies as time progresses. The phases of the particles try to drift away from each other but the mutual interaction between them reduces the phase difference again. This cyclic variation of the phase difference persists even in the asymptotic dynamics. It should be noted that there is a disparity between the experimental observations [Figs. 2(e) and 4(f)] and simulation results [Figs. 4(e) and 4(f)] for the counterrotating case. The reason for this discrepancy may be due to the rudimentary nature of our model which does not take into account the dependence of coupling on the rotation speed and direction of rotators [44]. Nonetheless, the model is able to qualitatively match the experimental observations.

VI. DISCUSSION

In the present work, rotational synchronization for corotating and counterrotating camphor ribbons has been presented. The pinned camphor ribbon rotates on the water surface due to a surface tension gradient introduced by the camphor layer. In this system, the initial direction of rotation, i.e., clockwise or counterclockwise, is determined by the random initial local perturbations. Once a ribbon begins to rotate in a particular direction, it sustains that motion. This is due to the fact that the asymmetric camphor distribution around the ribbons is now sustained by the motion itself. This acts as a positive feedback to the initial direction of motion, which was chosen randomly. The two camphor ribbons are coupled via a camphor layer around them. This is an indirect type of coupling. Each rotator leaves a trail of camphor when it passes the region in between the two pivots. This camphor layer influences the motion of the second rotator when it passes through the same region. This results in a repulsive coupling between the ribbons [25,42]. Lag synchronization for both corotating and counterrotating ribbons was experimentally observed. Synchronization is observed at a distance less than the sum of the span of the two ribbons, l_c. It was observed that counterrotating synchronization is more robust in comparison to its corotating counterpart.

To understand why the counterrotating mode of synchronization is more stable, the following intuitive argument can be given. Two corotating ribbons will move in opposite directions when they pass through the common region between the pivots. Since a camphor particle moves from high camphor concentration towards low camphor concentration (low surface tension to high surface tension), the rotators have to repeatedly reverse the direction of the camphor concentration gradient in the common region between the pivots. Since the repeated reversals of the concentration gradient require a finite amount of time, the rotators slow down in the common region. This slowdown translates to a greater chance of physical contact between them. In contrast, for counterrotating ribbons, the direction of the gradient created in the common region is the same for both the ribbons when they pass through it. Hence, they can traverse the common region relatively quickly and avoid physical contact.

The subtle difference between our results and mixed synchronization [33] needs to be emphasized. If the x and the y positions of the rotators are considered as independent state variables, our experimental observations (for counterrotating ribbons) can be considered as a manifestation of mixed synchronization.

Our simple model of two point rotators interacting via a repulsive Yukawa potential captures the essential features of the experiments. It is able to qualitatively reproduce the experimentally observed synchronization in both the co- and counterrotating modes based on the initial directions of rotations. We believe that the present table-top experimental system showing synchronized rotational motion through the dynamics of the fluidic surface constitutes an interesting contribution in the context of the growing field of active matter. Our future experiments will focus on exploring frustration type dynamics in more than two camphor ribbons.

ACKNOWLEDGMENTS

We would like to acknowledge financial support from DST (India) (Grant No. EMR/2016/000275). J.S. would like to thank MHRD and I.T. acknowledges CSIR, India, for financial support. Fruitful discussions with the Non-Linear Dynamics and the Statistical Mechanics laboratory, IITB, are also acknowledged.

[1] A. Pikovsky, M. Rosenblum, and J. Kurths, *Synchronization: A Universal Concept in Nonlinear Sciences*, Vol. 12 (Cambridge University Press, Cambridge, UK, 2003).

[2] D. K. Verma, H. Singh, A. Contractor, and P. Parmananda, J. Phys. Chem. A **118**, 4647 (2014).

[3] P. Kumar, D. K. Verma, P. Parmananda, and S. Boccaletti, Phys. Rev. E **91**, 062909 (2015).

[4] A. Biswas, D. Das, and P. Parmananda, Phys. Rev. E **95**, 042202 (2017).

[5] J. M. Cruz, M. Rivera, and P. Parmananda, Phys. Rev. E **75**, 035201 (2007).

[6] J. M. Cruz, A. Hernandez-Gomez, and P. Parmananda, Phys. Rev. E **75**, 055202(R) (2007).

[7] J. M. Cruz, J. Escalona, P. Parmananda, R. Karnatak, A. Prasad, and R. Ramaswamy, Phys. Rev. E **81**, 046213 (2010).

[8] S. Strogatz, *Sync: The Emerging Science of Spontaneous Order* (Penguin UK, London, 2004).

[9] A. B. Cawthorne, P. Barbara, S. V. Shitov, C. J. Lobb, K. Wiesenfeld, and A. Zangwill, Phys. Rev. B **60**, 7575 (1999).

[10] S. Nakata, K. Kayahara, M. Kuze, E. Ginder, M. Nagayama, and H. Nishimori, Soft Matter **14**, 3791 (2018).

[11] L. Glass, Nature (London) **410**, 277 (2001).

[12] T. Banerjee and A. Basu, Phys. Rev. E **96**, 022201 (2017).

[13] G. Novati, S. Verma, D. Alexeev, D. Rossinelli, W. M. van Rees, and P. Koumoutsakos, Bioinspiration Biomimetics **12**, 036001 (2017).

[14] N. Uchida, R. Golestanian, and R. R. Bennett, J. Phys. Soc. Jpn. **86**, 101007 (2017).

[15] Y. Man, W. Page, R. J. Poole, and E. Lauga, Phys. Rev. Fluids **2**, 123101 (2017).

[16] H. Guo, L. Fauci, M. Shelley, and E. Kanso, J. Fluid Mech. **836**, 304 (2018).

[17] K. Czolczynski, P. Perlikowski, A. Stefanski, and T. Kapitaniak, Commun. Nonlinear Sci. Numer. Simul. **17**, 3658 (2012).

[18] N. Chakrabarty, A. Jain, N. Lal, K. Das Gupta, and P. Parmananda, Chaos **27**, 013115 (2017).

[19] R. Toth, A. F. Taylor, and M. R. Tinsley, J. Phys. Chem. B **110**, 10170 (2006).

[20] C. Tomlinson, Proc. R. Soc. London **11**, 575 (1860).

[21] S. Nakata, Y. Iguchi, S. Ose, M. Kuboyama, T. Ishii, and K. Yoshikawa, Langmuir **13**, 4454 (1997).

[22] M. Nagayama, S. Nakata, Y. Doi, and Y. Hayashima, Physica D (Amsterdam, Neth.) **194**, 151 (2004).

[23] N. J. Suematsu, T. Sasaki, S. Nakata, and H. Kitahata, Langmuir **30**, 8101 (2014).

[24] G. Van der Mensbrugghe, Mém. Courronnés l'Acad. Roy. Sci. Belg. **34**, 1 (1869).

[25] H. Nishimori, N. J. Suematsu, and S. Nakata, J. Phys. Soc. Jpn. **86**, 101012 (2017).

[26] N. J. Suematsu, Y. Ikura, M. Nagayama, H. Kitahata, N. Kawagishi, M. Murakami, and S. Nakata, J. Phys. Chem. C **114**, 9876 (2010).

[27] Y. Hayashima, M. Nagayama, and S. Nakata, J. Phys. Chem. B **105**, 5353 (2001).

[28] Y. Hayashima, M. Nagayama, Y. Doi, S. Nakata, M. Kimura, and M. Iida, Phys. Chem. Chem. Phys. **4**, 1386 (2002).

[29] M. I. Kohira, Y. Hayashima, M. Nagayama, and S. Nakata, Langmuir **17**, 7124 (2001).

[30] S. Nakata, M. I. Kohira, and Y. Hayashima, Chem. Phys. Lett. **322**, 419 (2000).

[31] S. Nakata, Y. Doi, and H. Kitahata, J. Phys. Chem. B **109**, 1798 (2005).

[32] H. Kitahata, K. Kawata, S. Takahashi, M. Nakamura, Y. Sumino, and S. Nakata, J. Colloid Interface Sci. **351**, 299 (2010).

[33] A. Prasad, Chaos Solitons Fractals **43**, 42 (2010).

[34] Y. Koyano, M. Gryciuk, P. Skrobanska, M. Malecki, Y. Sumino, H. Kitahata, and J. Gorecki, Phys. Rev. E **96**, 012609 (2017).

[35] K. Iida, H. Kitahata, and M. Nagayama, Physica D (Amsterdam, Neth.) **272**, 39 (2014).

[36] N. J. Suematsu, S. Nakata, A. Awazu, and H. Nishimori, Phys. Rev. E **81**, 056210 (2010).

[37] See Supplemental Material at http://link.aps.org/supplemental/10.1103/PhysRevE.99.012204 for videos corresponding to unsynchronized (unsynchronized.mp4), corotating (co_rotating.mp4) and counterrotating (counter_rotating.mp4) camphor ribbons. In addition, video showing corotating (1.mp4) and counterrotating (2.mp4) ribbons' synchronization without a physical contact between the ribbons is provided. Also, the plot of the temporal behavior of the angular frequency of a single camphor ribbon is shown.

[38] D. Blair and E. Dufresne, Particle-tracking code available at http://physics.georgetown.edu/matlab (unpublished).

[39] J. C. Crocker and D. G. Grier, J. Colloid Interface Sci. **179**, 298 (1996).

[40] This gradual slowdown of rotation has also been mentioned previously in the isolated camphor rotators [34]. A single camphor ribbon also experiences a slowdown of rotations with time. Please see the Supplemental Material [37], where the plot of temporal behavior of the angular frequency of a single camphor ribbon is presented.

[41] Please see the Supplemental Material [37], which shows the corotating (1.mp4) and counterrotating (2.mp4) synchronization without a physical contact between the ribbons.

[42] S. Soh, K. J. Bishop, and B. A. Grzybowski, J. Phys. Chem. B **112**, 10848 (2008).

[43] A. Kaiser, K. Popowa, H. H. Wensink, and H. Löwen, Phys. Rev. E **88**, 022311 (2013).

[44] This reasoning was suggested to us by the anonymous referee.